ChemPubSoc Europe

DOI: 10.1002/chem.201606027

CHEMISTRY A European Journal Full Paper

Heterogeneous Catalysis

A Novel Green TiO_2 Photocatalyst with a Surface Charge-Transfer Complex of Ti and Hydrazine Groups

Lihong Tian,*[a, b] Jilian Xu,[c] Abrar Alnafisah,[a] Ran Wang,[b] Xinyu Tan,[d] Nathan A. Oyler,[a] Lei Liu,[c] and Xiaobo Chen*[a]

Abstract: The optical property of TiO_2 plays an important role in its various and promising photocatalytic applications. Previous efforts in improving its optical properties include doping with various metal and/or non-metal elements, coupling with other colorful semiconductors or molecules, and hydrogenating to crystalline/disordered core/shell nanostructures. Here, we report a beautiful green TiO_2 achieved by forming the charge-transfer complex of colorless hydrazine groups and surface Ti^{4+}, which extends the optical absorption into the near infrared region ($\approx$1100 nm, 1.05 eV). It shows an enhanced photocatalytic performance in hydrogen generation under simulated sunlight, and degradation of organic pollution under visible light due to an impurity state (about 0.28 eV) resulting in fast electron–hole separation and injection of electrons from the ligand to the conduction band of TiO_2. This study demonstrates an alternative approach to tune the optical, impurity state and photocatalytic properties of TiO_2 nanoparticles and we believe this will spur a wide interest in related materials and applications.

Introduction

Solar-driven photocatalytic hydrogen evolution and organic pollution removal are promising approaches to tackle the increasing renewable energy needs and environmental pollution concerns.[1] Titanium oxide is one of most attractive photocatalysts because of its numerous advantages and extraordinary photocatalytic activity.[2] However, TiO_2 has a wide band gap about 3.0–3.2 eV and only absorbs the ultraviolet (UV) light, which accounts for less than 5% of the natural sunlight spectra. In the past several decades, constant efforts have been made to increase its optical absorption from the UV to the visible or infrared light regions, which account for 43 and 52% of the solar spectrum, respectively. These efforts have included doping the lattice of TiO_2 with metal and/or non-metal atoms,[3] coupling with other colorful semiconductors or molecules,[4] loading with plasmonic noble-metal nanoparticles,[5] and hydrogenating to crystalline/disordered core/shell nanostructures.[6] For example, in the early 1990's, Choi et al. did a thorough study on metal doping in TiO_2 nanoparticles and found that in general its optical absorption was effectively shifted to the visible-light region, enhancing its photocatalytic activities, which were observed in the removal of various organic pollutants.[3a] Combinations of various metal doping were attempted and similar conclusions were obtained.[3a,7] The report of nitrogen doping in 2001 spurred a wide research interest in non-metal doping in TiO_2 and/or the combination of various metal/non-metal or non-metal/non-metal doping, resulting in various visible-light optical absorption and activities.[3b,c,8] Recent improvements of hydrogenation through the optical and photocatalytic activities has further stimulated research efforts in TiO_2 photocatalysis through optical property modifications.[5a] The hydrogenation process generally introduces a crystalline/disordered core/shell nanostructure, and a near-infrared absorption (onset absorption at 1200 nm in wavelength),[5a] a large shift in the valence-band edge, and large improvements in photocatalytic activities.[5a] Controlling the hydrogenation conditions further tune the optical properties and other physical and/or chemical characteristics for photocatalysis.[9] The crystalline/disordered core/shell nanostructure also benefits the charge separation process in photocatalysis, with similar functions to the p–n heterojunctions.[10] Combinations of metal/non-metal doping, and hydrogenation have been recently pursued to take advantage of both approaches and promising results are frequently reported.[11] These approaches have also been expanded to many other material sys-

[a] Prof. L. Tian, Prof. A. Alnafisah, Prof. N. A. Oyler, Prof. X. Chen
Department of Chemistry, University of Missouri–Kansas City
Kansas City, Missouri 64110 (USA)
E-mail: tian7978@hubu.edu.cn
chenxiaobo@umke.edu

[b] Prof. L. Tian, R. Wang
Department Hubei Collaborative Innovation Center for Advanced Organochemical Materials
Ministry of Education Key Laboratory for the Synthesis and Applications of Organic Functional Molecules, Hubei University
Wuhan, 430062 (P. R. China)

[c] Dr. J. Xu, Prof. L. Liu
State Key Laboratory of Luminescence and Applications
Changchun Institute of Optics, Fine Mechanics and Physics
Chinese Academy of Sciences, Changchun, 130033 (P. R. China)

[d] Prof. X. Tan
College of Science, China Three Gorges University
Yichang, 443002 (P. R. China)

Supporting information for this article can be found under: http://dx.doi.org/10.1002/chem.201606027.

tems to gain better optical and photocatalytic properties.[12] Despite this steady progress, the optical properties of TiO_2 is still far from satisfactory, and new approaches are desired to provide in tuning the optical and photocatalytic properties of TiO_2 and other materials.

Forming multiple ring coordination of bidendate benzene derivatives with surface Ti-atoms was reported to improve the optical and charge-separation properties of TiO_2 nanocrytals, including vitamin C,[13] catecholate,[14] salicylic acid,[15] and gallic acid.[16] In those cases, electrons transferred from coordinated ligands to the conduction band of TiO_2, inducing the red shift of the absorption edge and the holes located in the surface complex. In this work, we first present a bidendate ligand containing nitrogen atoms (hydrazine molecule) to modify the optical properties and introduce an impurity state into TiO_2 photocatalysts, distinct from the previous benzene derivatives. The green TiO_2 nanocrystal displays excellent photocatalytic activity for both hydrogen evolution under simulated sunlight and organic pollutant removal under visible light. Thus, this study successfully demonstrates a new substitution in steering the optical, impurity state, and photocatalytic properties of TiO_2.

Results and Discussion

Figure 1 A shows a photo of the green TiO_2 sample obtained by the condensation reaction in the presence of hydrazine monohydrochloride; notably, white TiO_2 was obtained in the absence of hydrazine monohydrochloride. The green TiO_2 displayed an enhanced absorption both in the ultraviolet- and visible-light region as compared to white TiO_2. A small peak around 700 nm was observed for green TiO_2, likely ascribed to the charge transfer between the hydrazine molecule and Ti atoms. According to the Kubelka–Munk formula,[17] a narrowed optical band gap of green TiO_2 (2.84 eV) was achieved compared with that of white TiO_2 (3.15 eV). Moreover, the green TiO_2 extended the absorption to about 1100 nm (1.05 eV) in Figure 1 B.

The XRD patterns of the white and green TiO_2 are shown in Figure 1 C. The white TiO_2 displayed a typical anatase structure (JCPDS no. 21-1272) with diffraction peaks around 25.2, 37.9, 47.8, 54.3, and 62.7° in a 2 theta value, corresponding to the (101), (004), (200), (105)/(201), and (204) plane, respectively. However, the green TiO_2 had a stronger and wider (101) peak than white TiO_2 along with a broad background, indicating a preferential [101] growth direction of green TiO_2 and much smaller particle size. This large background possibly came from a large amount of amorphous phase without a long-range crystallinity on green TiO_2. The transmission electron microscopy (TEM) image in Figure 1 D confirmed the green TiO_2 had a very small particle size around 10 nm, although aggregation was also seen. The high-resolution TEM (HRTEM) image in Figure 1 E further indicated the green TiO_2 nanocrystals had a high crystallinity from the clear and well-resolved crystal lattices. The lattice spacing of 0.352 nm corresponded to the (101) plane of anatase TiO_2. The strong Raman peaks around 164.2, 422.5, 536.5, and 662.3 cm^{-1} indicated a crystalline anatase phase for both the white and green TiO_2 in Figure 1 F.[14] The

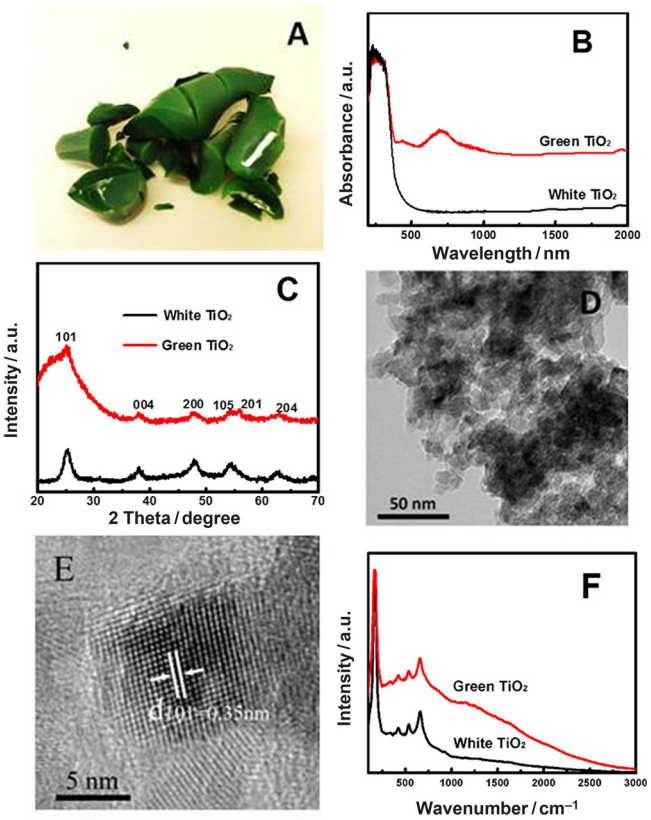

Figure 1. (A) A digital picture of the green TiO_2; (B) UV/Vis diffusion reflection spectra and (C) XRD patterns of the white and green TiO_2; (D) TEM and (E) HRTEM images of the green TiO_2; and (F) Raman spectra of the white and green TiO_2.

difference was that green TiO_2 had a much stronger photoluminescence background, indicating that the green TiO_2 had more defects or amorphous phases than the white TiO_2, identical to the XRD results.

To determine what induced the beautiful green color and defects on TiO_2, we analyzed the surface chemical properties using X-ray photoelectron spectroscopy (XPS), ^{1}H NMR, and Fourier transform infrared (FTIR) spectroscopy. The white and green TiO_2 had similar XPS spectra with signals from titanium, oxygen, carbon, and a trace amount of nitrogen in Figure 2 A. The carbon signal from the carbon deposition in the XPS measurement was calibrated to 284.6 eV for the binding energy. The content of nitrogen apparently increased further on the surface of the green TiO_2 than that on the white TiO_2. From Figure 2 B and C, no distinct change was observed in Ti 2p and O 2p spectra in both the white and green TiO_2. Two peaks at 458.4 and 464.1 eV were ascribed to the Ti 2p3/2 and Ti 2p1/2 of Ti^{4+} ions,[2,4c,10b] and no Ti^{3+} or other lower valence species was observed because no shoulders were observed at lower binding energy.[18] One main peak at 530.0 eV and a small shoulder peak at 532.0 eV were attributed to the lattice oxygen and some hydroxyl groups, likely from adsorbed water on the surface, respectively.[10b] However, the N 1s XPS spectra of green TiO_2 varied from that of white TiO_2 in Figure 2 D. The main peak around 402.4 eV was likely from the nitrogen in the

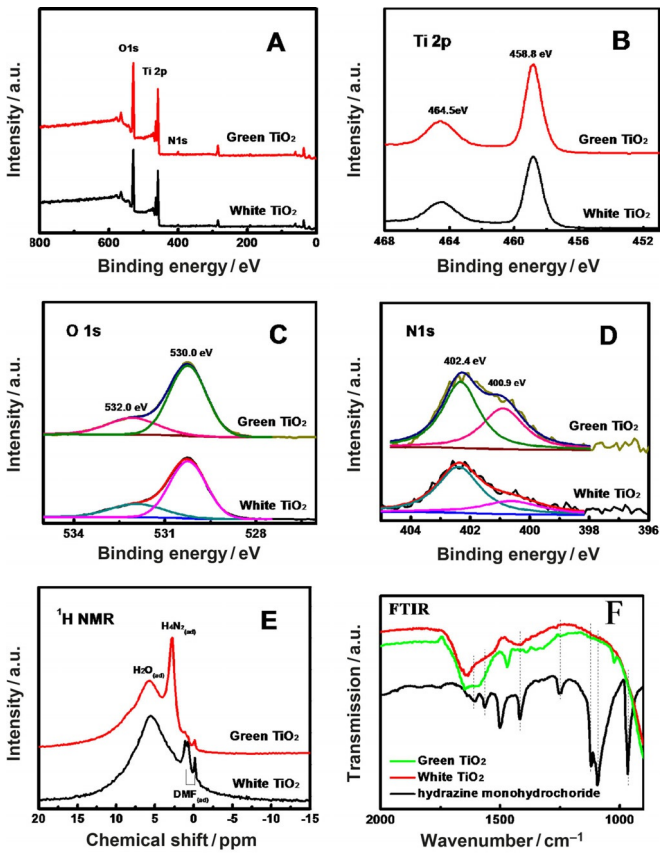

Figure 2. (A) The survey, (B) Ti 2p; (C) O 1s; (D) N 1s core-level XPS spectrum of white and green TiO_2; (E) solid-state 1H NMR; and (F) FT-IR spectra of the different samples.

adsorbed organic molecule. A weak peak at around 400.6 eV was likely associated with the coordinated N atoms joining in TiO_2 lattice,[18] which appeared at a higher binding energy of 400.9 eV in the green TiO_2. This suggested an electron deviation existed from coordinated hydrazine to TiO_2. Meanwhile, the intensity dramatically increased compared to that of white TiO_2, indicating that the hydrazine molecule was more inclined to coordinate with Ti atoms than with DMF, which terminated the periodic structure of TiO_2. The solid-state ^{1}H NMR spectra of the white and green TiO_2 are shown in Figure 2E. The comparison to those of pure TiO_2 (Degussa P25) and pure hydrazine monohydrochloride is displayed in Figure S1 in the Supporting Information. Both the white and green TiO_2 had a large broad peak near 5.43 ppm as well as two weak peaks around 1.11 and 0.0 ppm, which were from the absorbed H_2O and -CH_3 in the adsorbed DMF solvent on the surface, respectively. However, a strong sharp peak near 2.80 ppm, lower than that of hydrazine monohydrochloride (3.08 ppm), was observed in green TiO_2. This slight shift is likely ascribed to the N in hydrazine substituting for the lattice O (XPS result). Accompanied with the appearance of the hydrazine molecule, the intensities of the peaks from the adsorbed water and solvent decreased in the green TiO_2 compared to the white TiO_2.

The comparison of the FTIR spectra of hydrazine monohydrochoride, white TiO_2, and green TiO_2 is shown in Figure 2F. For white TiO_2, the peaks at 1650 and 1420 cm^{-1} were likely from the stretching of C=O groups and the bending variation of -CH_3 from the adsorbed DMF on the surface.[20] Nevertheless, the spectrum of green TiO_2 was very distinct from that of white TiO_2, displaying a band at 1600 cm^{-1} and a peak at 1470 cm^{-1} from the N–H bending vibration in the hydrazine molecules. A weak peak at 1026 cm^{-1} was ascribed to the -NH_2 rocking vibration. Compared with the spectrum of hydrazine monohydrochoride (1608, 1500, and 1094 cm^{-1}), these peaks shifted to a much lower wavenumber, indicating hydrazine molecules were likely coordinating with surface Ti-atoms of TiO_2. The result is also consistent with the XPS and NMR measurements. Thus, based on the above measurements, we confirmed that the N-atom in hydrazine coordinated the Ti^{4+} to form a charge-transfer bond, which resulted in the absorption at 700 nm in the UV/Vis spectra. This gave TiO_2 a beautiful green appearance. It should be noted that the substitution from DMF did not induce a color change and the white TiO_2 was still obtained, indicating no charge-transfer bonding formation.

A first-principles density functional theory (DFT) calculation was conducted to investigate the effect of hydrazine on the band structure. We calculated the model of a hydrazine molecule coordinated on the (001) surface, because XRD and HRTEM results showed that the hydrazine molecule led to a predominant growth of the green TiO_2 as well as the [101] direction. Firstly, if the N-atoms in impurity states were located within the valence band instead of in the band gap, a large lattice deformation should be observed (Figure S2–S4 in the Supporting Information), which was not consistent with XRD and TEM. However, when N-atoms in hydrazine substituted the surface O-atoms and coordinated with Ti-atoms (see the surface model of hydrazine on the TiO_2 surface in Figure 3A), two impurity bands in the band gap formed: a high-energy state about 1.8 eV above the surface valence-band maximum, and a low-energy state mixed with the surface states in the valence band (Figures 3B and S5). In this case, the electrons in the high-energy impurity state were localized in the hydrazine molecule, and those in the low-energy impurity state distributed on the TiO_2 surface and the hydrazine molecule (Figure 3C).

The photocatalytic activity of H_2 evolution under both visible and simulated solar light was evaluated in comparison to the white TiO_2 and commercial Degussa P25. Unfortunately, green TiO_2 had very low H_2-evolution activity under visible light (results not shown here), but it showed 2.9- (3.27 mmol h^{-1} g^{-1}) and 2.3-fold higher activity than that of the white TiO_2 (1.14 mmol h^{-1} g^{-1}) and P25 (1.44 mmol h^{-1} g^{-1}) at pH 1 under simulated solar light, as shown in Figures 4A and S6A. In fact, a pH-robust activity was observed across the entire pH range, with an activity between 2.33 and 3.94 mmol h^{-1} g^{-1} at the pH values of 1–13 (Figures 4B and S6B–H), indicating green TiO_2 exhibited a high photocatalytic activity in generating H_2 in both acid and basic solutions.

Nevertheless, it is interesting that green TiO_2 presented a much better visible-light ($\lambda > 400$ nm) photocatalytic activity on the degradation of organic pollutants than the white TiO_2. As shown in Figure 4C, the green TiO_2 showed 7.6- and 1.7-

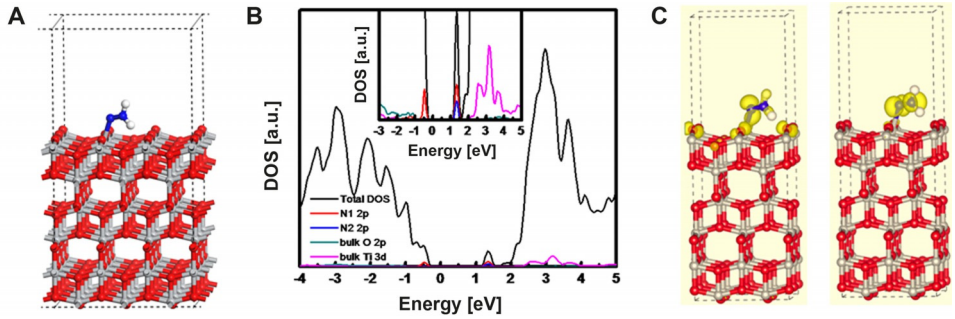

Figure 3. (A) The surface model of the green TiO_2; (B) DOS (Density of States) of the possible (001) surface of the green TiO_2; (C) local charge density of hydrazine states: low-energy (left) and high-energy (right) impurity states.

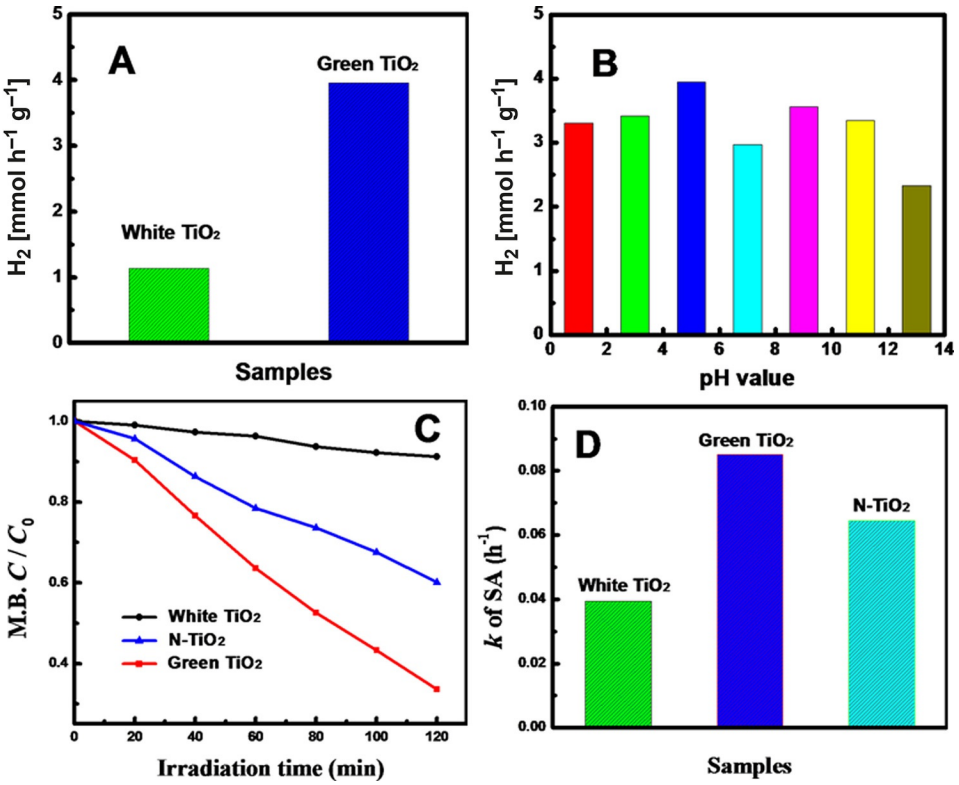

Figure 4. (A) Photocatalytic hydrogen generation with the white and green TiO_2; (B) the photocatalytic hydrogen generation with the green TiO_2 at various pH values under simulated sunlight irradiation, and photocatalytic degradation of MB (C) and SA (D) under visible light ($\lambda > 400$ nm).

fold higher photocatalytic activity than those of the white TiO_2 and *N*-TiO_2, respectively, in decomposing methyl blue (MB). Moreover, the degradation rate constant (*k*) of colorless salicylic acid (SA) on green TiO_2 was 0.0852 h^{-1}, which was 2.2 and 1.3 times that of white TiO_2 (0.0393 h^{-1}) and *N*-TiO_2 (0.0645 h^{-1}), respectively, as shown in Figure 4D. The effect of initial concentration of MB and SA on the *k* value has also been investigated in Figure S7 (see the Supporting Information). The optimal concentration of MB was about 10 mg L^{-1}, and the degrading rate constant was 9.15×10^{-3} min^{-1} (Figure S7A), but *k* decreased with increasing initial concentration of SA (Figure S7B). Figure S8 shows that green TiO_2 was stable and still maintained excellent activity for the photocatalytic degrading MB after four successive recycling runs.

Generally, the photocatalytic H_2 evolution and organic degradation depended on the conduction band (CB) electrons reduction and radical oxidation, respectively. We analyzed the change of band structure and charge transfer of white and green TiO_2 to determine the intrinsic reason of the enhanced photocatalytic activity for green TiO_2. The Mott–Schottky plots of the white and green TiO_2 give the plots of C^{-2} and *E* in the potential range of −1.2–1.0 V versus Ag/AgCl (Figure 5A). The flat band potential was −0.75 and −0.98 V versus Ag/AgCl for the white and green TiO_2, and the corresponding CB potential of white and green TiO_2 was −0.53 and −0.76 eV (vs. normal hydrogen electrode), respectively. Combining with the optical band gap, the valence band (VB) potential was 2.62 and 2.08 eV for white and green TiO_2, respectively. Thus, the impur-

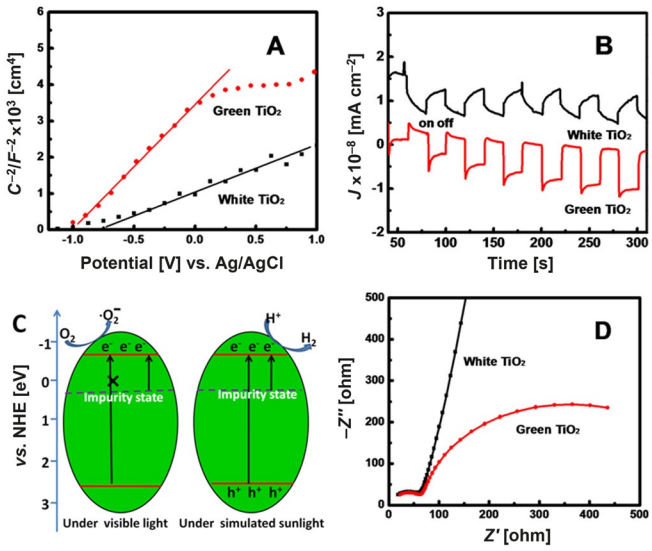

Figure 5. (A) Mott–Schottky plots of the white and green TiO_2; (B) the transient photocurrent responses in 0.5 M Na_2SO_4 aqueous solution; (C) the proposed photocatalytic mechanism on green TiO_2; and (D) EIS Nyquist plots.

ity state was located at 0.28 eV according to the DFT calculations (1.8 eV above the valence band) and the UV/Vis DRS results. In Figure 5B, the transient photocurrent increased sharply once the light illumination was activated, but dropped to a minimum in the dark. White TiO_2 displayed the steady and reproducible on–off cycles for chopped illumination time. However, an interesting phenomenon appeared on the green TiO_2, and the opposite photocurrent was produced under the identical experimental condition. When a positive bias potential (0.1 V) was applied, the photocurrents became positive, as shown in Figure S9 in the Supporting Information. According to the DFT theory calculation results, we inferred that the negative photocurrent likely came from the electrons at the coordinated hydrazine molecule with a high-energy state transferred to the CB of green TiO_2. Thus, a scheme was proposed to help understand the charge transfer and the enhanced photocatalytic activity of green TiO_2 in Figure 5C. The visible light is not enough to excite electrons from the VB to CB (−0.76 eV) of green TiO_2, but electrons located at the impure high-energy state can be excited to the CB of TiO_2. Electrons can react with O_2 to superoxide radicals, oxidizing the organic contaminant. However, under simulated sunlight, these electrons combined with those coming from the VB of green TiO_2 contributed to the H_2 evolution.

The Electrochemical impedance (EIS) spectra of the white and green TiO_2 are shown in Figure 5D. According to the Grätzel's report,[21] the high-frequency feature was attributed to the charge transfer at the counter electrode, whereas the response in the intermediate-frequency region was associated with the electron transport in the working electrode, and the low-frequency region indicated diffusion in the electrolyte. The white TiO_2 had a semicircle in high frequency from the charge transfer at the counter Pt electrode along with a short straight line at lower frequency from the diffusion-directed process. Although the green TiO_2 showed one semicircle for the charge transfer at the counter Pt electrode in the high-frequency region, and another semicircle at intermediate frequency due to the electron transfer between TiO_2 and hydrazine molecules adsorbed on the surface, the straight line from the diffusion-directed process was not observed, likely due to the dominating charge transfer process over the diffusion process at low frequency. This indicated the surface hydrazine groups can also hamper the electron–hole recombination and lead to a higher photocatalytic activity. The N_2 adsorption–desorption isotherm curves of the white and green TiO_2 are shown in Figure S10 and S11 in the Supporting Information, respectively. Both of them correspond to the classical type IV curve with an H2 hysteresis loop, suggesting the presence of a mesoporous framework. Figure S11 suggested the average pore size was about 3.69 nm. These mesopores allowed the rapid diffusion of gas and other photocatalytic reactants, enhancing the rate of photocatalytic reaction. A comparison of the Brunauer–Emmett–Teller (BET) surface and pore size of the white and green TiO_2 is displayed in Table S1. The green TiO_2 had a larger BET surface area (142.8 $m^2 g^{-1}$) than the white TiO_2 (104.5 $m^2 g^{-1}$), but the average pore size had no apparent change. The lager surface area of the green TiO_2 benefited the adsorption of pollution and photocatalytic activity. Thus, green TiO_2 showed a higher photocatalytic H_2-evolution performance under simulated solar light and degrading environmental contaminants under visible light over white TiO_2 due to the electron transfer at a high energy state, efficient separation of electrons and holes, and a large BET surface area.

Conclusion

We have demonstrated the coordination of a hydrazine molecule to the surface of titanium atoms to change the optical property and band structure of a TiO_2 photocatalyst. An impurity state was created and a charge transfer induced TiO_2 with beautiful green color. The green TiO_2 showed a pH-robust activity across the entire pH range, with 2.9 (3.27 mmol $h^{-1} g^{-1}$) and 2.3-fold higher activity than that of the white TiO_2 (1.14 mmol $h^{-1} g^{-1}$) and P 25 (1.44 mmol $h^{-1} g^{-1}$), respectively, at pH 1 under simulated solar light, due to electron donation from hydrazine to the CB of TiO_2 and the efficient inhibition of electrons and holes. Moreover, it also had high visible-light performance on the degradation of organic contaminants with 7.6 times activity in decomposing MB and 2.2 times activity in decomposing colorless SA as that of the white TiO_2, respectively, as a result of the contribution of the impurity band at high-energy state and a large BET surface area. Distinct from previous doping, hydrogenating, or coupling efforts, this study thus presents an alternative approach to improve the optical and photocatalytic properties of TiO_2. The findings may also be applied to other photocatalytic materials and applications.

Experimental Section

Synthesis of green TiO_2 colloidal nanocrystal: The target material was synthesized by a solvothermal method. Typically, 3 mL titanium isopropoxide was slowly added to 35 mL of DMF at ambient

conditions by vigorously stirring, producing a completely transparent solution. A desired amount of hydrazine monohydrochloride was added into the above solution with the molar ratio of Ti:N_2H_5Cl being 0.5–2.5, then the solution was transferred into a Teflon-lined, stainless steel autoclave at different temperatures of 140–200 °C for 12 h, obtaining a green powder. The products were washed with anhydrous ethanol and deionized water, then dried at 100 °C for overnight. The pristine TiO_2 was prepared by the same method without adding hydrazine monohydrochloride.

Characterization: Crystal phases of the catalysts were tested on a Rigaku Miniflex X-ray Diffractometer (XRD) with a CuKα (λ = 0.15418 nm) radiation source. The morphology and structure were studied on a high-resolution transmission electron microscope (TEM, FEI Tecnai F20 STEM) with the electron accelerating voltage of 200 kV. A small amount of powder sample dispersed in ethanol was dropped onto a thin holey carbon film, and dried overnight before TEM measurement. The surface area was calculated by the BET method from nitrogen adsorption–desorption data, which was measured on a Quanta-chrome autosorb-1 automated gas sorption system at 77 K. XPS measurements were carried out on a Kratos Axis 165 X-ray photoelectron spectrometer with an Al/Mg dual-anode X-ray source, using a photon beam of 1486.6 eV, and all the spectra were calibrated to the C 1s peak at 284.6 eV. The reflectance spectra were collected with a UV-3600 UV/Vis spectrometer with a fiber optical reflectance unit. $BaSO_4$ power was used as the reference material. The FTIR spectra were collected using a Thermo-Nicolet iS10 FT-IR spectrometer with an attenuated total reflectance (ATR) unit. Sample powders were pressed onto the ZnSe crystal of the ATR unit, and the measurements were performed in air at room temperature. The Raman spectra were collected on an EZRaman-N bench top Raman spectrometer. The Raman spectrometer was equipped with a diode laser and the excitation wavelength was 785 nm. The spectrum range was from 100–3000 cm^{-1}. All ^1H NMR experiments were performed on an 8.45 tesla Oxford magnet with a three channel Tecmag Apollo NMR console, using a home-built, doubly tuned, MAS solid-state NMR probe with a 3.2 mm stator assembly from Revolution NMR. The magic angle spinning rate was 8 kHz, the proton excitation pulse during the Bloch decay experiment was about 50 kHz, and each spectrum was acquired with 256 scans. The spectra were externally referenced to adamantane. NMR spectra were acquired of the both samples as well as an empty rotor to measure the hydrogen present. The contribution of the empty rotor was then subtracted to obtain the information from the samples which was further scaled by the mass of samples to give a quantitatively accurate spectrum.

Theoretical calculation: All our calculations were based on DFT within PBE+U approach (Perdew-Burke-Ernzerhof). U = 10.0 eV was applied to the Ti 3d states to deal with the band gap underestimation. In this scheme, the calculated band gap of bulk anatase TiO_2 was 3.08 eV (the experimental lattice parameters of a = 3.7842 and c = 9.5146 are used), which is approximate with the experimental value of 3.2 eV. A (2×2) slab model was constructed to represent the (001) surface of anatase TiO_2, containing six O-Ti-O layers and a vacuum region of larger than 15 Å. During structural relaxation, the bottom trilayer is fixed to simulate the bulk environment, and all other layers are allowed to relax. The Brillouin zones are sampled with a (3×3×1) Monkhorst–Pack mesh. The atomic positions are fully relaxed until the residual forces are less than 0.01 eV/Å.

Photoelectrochemical measurement: Photocurrents were measured on an electrochemical analyzer (CHI 660C) in a standard two-electrode system with the as-prepared samples as the working electrodes and a Pt plate as the counter electrode. A 150 W Xenon lamp was used as the light source and the electrolyte was 0.5 mol L^{-1} Na_2SO_4 aqueous solution. For the working electrode, 10 mg of sample was dispersed in 4 mL ethanol to obtain a suspension. Then, the suspension was coated onto a glassy carbon electrode and dried in an oven. EIS spectra of all samples were collected with a scan rate of 5 mVs^{-1}, at the frequency of 5 Hz and of 0.1 V initial voltage which was obtained by measuring the open circuit potential. For the working electrode, a sample (10 mg) was dispersed in ethanol (1 mL) to obtain a slurry. Then, eight drops of the slurry was coated onto a glassy carbon electrode and dried in high pressure sodium lamp. A Pt wire was used on the counter electrode.

Photocatalytic hydrogenation evolution test: 20 mg of samples was dispersed with sonication in 100 mL (volume ratio = 1: 1) of a CH_3CH_2OH/ H_2O solution. HCl and NaOH were used to adjust the pH value of solution. A suitable amount of H_2PtCl_6 solution was added into the solution to make 0.6 wt% Pt on the photocatalysts. Prior to the tests, the reactor was sealed and purged with Ar gas for 20 min to ensure the removal of air. The reaction was conducted with a solar simulator under magnetic stirring. The solar simulator (81094, Newport) has a 150 W Xe lamp with an AM 1.5 air mass filter to simulate natural sunlight. At a 2 h interval, the gaseous reaction products were monitored by a gas chromatography (Agilent MicroGC) equipped with a thermal conductivity detector.

Photocatalytic degradation of contaminants: The photocatalytic degradation of methyl blue (MB) and salicylic acid (SA) was performed under visible-region irradiation using a 300 W Xe lamp (CEL-HXF300) with a UV light filter, which cuts off the short wavelength light (< 400 nm). In a typical run, 10 mg of photocatalysts was suspended in 50 mL of 10 mg L^{-1} MB or 5×10^{-5} mol L^{-1} SA aqueous solution. Prior to light irradiation, the suspension was sonicated for 30 min and stirred for an hour in the dark to ensure the establishment of the adsorption/desorption equilibrium on the catalyst surface. Then the solution was placed in a quartz reaction and stirred with a magnetic stirrer. At given time intervals, aliquot 4 mL solution was taken out. After the suspended catalysts were removed by centrifugation, the concentration of MB and SA was determined with a UV/Vis spectrophotometer (Cary 60).

Acknowledgements

X.C. acknowledges the support from the College of Arts and Sciences, University of Missouri–Kansas City, and the University of Missouri Interdisciplinary Intercampus (IDIC) Program. L.T. thanks the National Natural Science Foundation of China (no. 51302072) and the China Scholarship Council for financial support.

Conflict of interest

The authors declare no conflict of interest.

Keywords: charge-transfer · hydrazine · hydrogen evolution · photocatalysis · titanium dioxide

[1] a) M. R. Hoffmann, S. T. Martin, W. Choi, D. W. Bahnemannt, *Chem. Rev.* **1995**, *95*, 69–96; b) X. Chen, S. Shen, L. Guo, S. S. Mao, *Chem. Rev.* **2010**, *110*, 6503–6570.

[2] X. Chen, S. S. Mao, *Chem. Rev.* **2007**, *107*, 2891–2959.

[3] a) W. Choi, A. Termin, M. R. Hoffmann, *Angew. Chem.* **1994**, *106*, 1148 – 1149; b) G. Liu, L. C. Yin, J. Wang, P. Niu, C. Zhen, Y. Xie, H. M. Cheng, *Energy Environ. Sci.* **2012**, *5*, 9603 – 9610; c) B. Liu, L. M. Liu, X. F. Lang, H. Y. Wang, X. W. Lou, E. S. Aydil, *Energy Environ. Sci.* **2014**, *7*, 2592 – 2597.

[4] a) H. Li, H. Yu, X. Quan, S. Chen, H. Zhao, *Adv. Funct. Mater.* **2015**, *25*, 3074 – 3080; b) S. Bai, L. Wang, X. Chen, J. Du, Y. Xiong, *Nano Res.* **2015**, *8*, 175 – 183; c) K. Ma, O. Yehezkeli, D. W. Domaille, H. H. Funke, J. N. Cha, *Angew. Chem.* **2015**, *54*, 11490 – 11494.

[5] a) K. Awazu, M. Fujimaki, C. Rockstuhl, J. Tominaga, H. Murakami, Y. Ohki, N. Yoshida, T. Watanabe, *J. Am. Chem. Soc.* **2008**, *130*, 1676 – 1680; b) S. Linic, P. Christopher, D. B. Ingram, *Nat. Mater.* **2011**, *10*, 911 – 921.

[6] a) X. Chen, L. Liu, P. Y. Yu, S. S. Mao, *Science* **2011**, *331*, 746 – 750; b) A. Naldoni, M. Allieta, S. Santangelo, M. Marelli, F. Fabbri, S. Cappelli, C. L. Bianchi, R. Psaro, V. D. Santo, *J. Am. Chem. Soc.* **2012**, *134*, 7600 – 7603; c) A. T. Xia, C. Zhang, N. A. Oyler, X. Chen, *Adv. Mater.* **2013**, *25*, 6905 – 6910.

[7] a) W. Choi, A. Termin, M. R. Hoffmann, *J. Phys. Chem.* **1994**, *98*, 13669 – 13679; b) N. Serpone, D. Lawless, J. Disdier, J. M. Herrmann, *Langmuir* **1994**, *10*, 643 – 652; c) A. L. Linsebigler, G. Lu, J. T. Yates Jr., *Chem. Rev.* **1995**, *95*, 735 – 758.

[8] a) R. Asahi, T. Morikawa, T. Ohwaki, K. Aoki, Y. Taga, *Science* **2001**, *293*, 269 – 271; b) Y. Cong, J. Zhang, F. Chen, M. Anpo, D. He, *J. Phys. Chem. C* **2007**, *111*, 10618 – 10623; c) X. Chen, C. Burda, *J. Am. Chem. Soc.* **2008**, *130*, 5018 – 5019; d) S. In, A. Orlov, R. Berg, F. García, S. Pedrosa-Jimenez, M. S. Tikhov, D. S. Wright, R. M. Lambert, *J. Am. Chem. Soc.* **2007**, *129*, 13790 – 13791.

[9] a) Y. H. Hu, *Angew. Chem. Int. Ed.* **2012**, *51*, 12410 – 12412; *Angew. Chem.* **2012**, *124*, 12579 – 12581; b) G. Wang, H. Wang, Y. Ling, Y. Tang, X. Yang, R. C. Fitzmorris, C. Wang, J. Z. Zhang, Y. Li, *Nano Lett.* **2011**, *11*, 3026 – 3033.

[10] a) J. Cai, Y. Zhu, D. Liu, M. Meng, Z. Hu, Z. Jiang, *ACS Catal.* **2015**, *5*, 1708 – 1716; b) T. Xia, C. Zhang, N. A. Oyler, X. Chen, *Adv. Mater.* **2013**, *25*, 6905 – 6910.

[11] W. Wang, C. Lu, Y. Ni, M. Su, Z. Xu, *Appl. Catal. B* **2012**, *127*, 28 – 35.

[12] a) J. Hou, H. Cheng, C. Yang, O. Takeda, H. Zhu, *Nano Energy* **2015**, *18*, 143 – 153; b) V. K. Sharma, G. D. Varma, *J. Appl. Phys.* **2007**, *102*, 056105; c) C. Yao, B. Wei, H. Ma, H. Li, L. Meng, X. Zhang, Q. Gong, *J. Power Sources* **2013**, *237*, 295 – 299.

[13] T. Rajh, J. M. Nedeljkovic, L. X. Chen, O. Poluektov, M. C. Thurnauer, *J. Phys. Chem. B* **1999**, *103*, 3515 – 3519.

[14] S. Higashimoto, T. Nishi, M. Yasukawa, M. Azuma, Y. Sakata, H. Kobayashi, *J. Catal.* **2015**, *329*, 286 – 290.

[15] T. D. Savić, Z. V. Šaponjić, M. I. Čomor, J. M. Nedeljković, M. D. Dramićanin, M. G. Nikolić, D. Ž. Veljković, S. D. Zarić, I. A. Janković, *Nanoscale* **2013**, *5*, 7601 – 7612.

[16] I. Vukoje, T. Kovac, J. Dzunuzovic, E. Dzunuzovic, D. Loncarevic, S. P. Ahrenkiel, J. M. Nedeljkovic, *J. Phys. Chem. C* **2016**, *120*, 18560 – 18569.

[17] M. A. Butler, *J. Appl. Phys.* **1977**, *48*, 1914 – 1920.

[18] F. B. Li, X. Z. Li, *Appl. Catal. A* **2002**, *228*, 15 – 27.

[19] a) T. Zhang, M. Xu, L. He, K. Xi, M. Gu, Z. Jiang, *Carbon* **2008**, *46*, 1782 – 1791; b) Y. Aoi, K. Sakurada, E. Kamijo, *Appl. Phys. A* **2004**, *79*, 1533 – 1536.

[20] S. F. Wang, T. Furuno, Z. Cheng, *J. Wood Sci.* **2003**, *49*, 371 – 376.

[21] Q. Wang, J. E. Moser, M. Grätzel, *J. Phys. Chem. B* **2005**, *109*, 14945 – 14953.

Manuscript received: December 26, 2016
Accepted Article published: January 29, 2017
Final Article published: March 28, 2017